Hindawi
Shock and Vibration
Volume 2019, Article ID 2092796, 18 pages
https://doi.org/10.1155/2019/2092796

Research Article

Numerical Study of Separation Characteristics of Piston-Type Explosive Bolt

Yanhua Li,[1] **Jingcheng Wang**,[1] **Shihui Xiong**,[1] **Li Cheng**,[1] **Yuquan Wen**,[1] **and Zhiliang Li**[2]

[1]*State Key Laboratory of Explosion Science and Technology, Beijing Institute of Technology, Beijing 100081, China*
[2]*CNGC Xi'an Qinghua, North Special Energy Group Co. Ltd., Xi'an, China*

Correspondence should be addressed to Yuquan Wen; wyquan@bit.edu.cn

Received 26 October 2018; Revised 4 January 2019; Accepted 22 January 2019; Published 13 February 2019

Academic Editor: Salvatore Russo

Copyright © 2019 Yanhua Li et al. This is an open access article distributed under the Creative Commons Attribution License, which permits unrestricted use, distribution, and reproduction in any medium, provided the original work is properly cited.

An explosive bolt is a simple, highly reliable, and efficient pyrotechnic release device widely used in spacecraft and rocket launchers. High shock transient response is generated during the separation of a release device, which tends to damage the nearby micromechanism and hardware. The purpose of this article is to predict the shock response of an explosive bolt. In this paper, the separation process of a piston-type explosive bolt is simulated by using a hydrocode named AUTODYN and the influence of the charge amount on separation time, separation speed, and separation shock is analyzed. Results show that piston-type explosive bolts obey a tensile fracture mechanism and that the critical charge amount for separation is 354–398 mg of PETN. The separation shock of such an explosive bolt mainly includes two aspects: the shock caused by explosive detonations and the impact of the piston at the end of the stroke. As the charge amount increases, the separation time decreases, the speed of the piston and screw increases first and then decreases, and the separation shock first increases and then stabilizes. On a simple aluminum plate, the shock response decreases as the distance from the shock source increases, obeying the power function attenuation law.

1. Introduction

An explosive bolt is a simple, highly reliable, and efficient pyrotechnic release device widely used in the aerospace industry [1, 2]. Various types of explosive bolts have been designed, including "ridge-cut" [3, 4], fragmenting-type [5], piston-type [6, 7], shear-type [8, 9], and shear pin-type explosive bolts [10], among others. The action of explosive bolts inevitably induces high-frequency and high-amplitude transient shock, known as pyroshock, which rarely causes structure failure. However, it can easily damage nearby electronics, optics, relays, and magnetic components and can ultimately lead to overall failures of space missions [11]. To mitigate damage from pyroshock, previous studies mainly focused on the characteristics of pyroshock propagation and damage evaluation through a large number of tests [12, 13], and numerous test standards [14–17] and experimental simulation methods [18] have been published. Past shock-preventing measures have also mainly focused on isolation from shock propagation paths and instrument installation [19, 20].

Protective measures requiring additional structures have been limited with the application of lightweight space structures, such as small satellites and deep-space probes, and measures to mitigate the shock from shock-generated sources are favored. Accurate analysis of the separation mechanism of pyrotechnic separation devices is a prerequisite for understanding shock generation characteristics. Owing to the highly nonlinear nature of combustion and explosion, it is difficult to accurately analyze in theory and monitor internal dynamic parameters (such as internal pressure, stress, and energy). In recent years, nonlinear dynamics simulation software has undergone rapid development. To solve the problems of high strain and large deformation in explosive shocks, new algorithms, such as fluid-structure interaction and smoothed particle hydrodynamics (SPH), have been developed along with many complex material models. These provide a practical way of

analyzing separation characteristics of pyrotechnic separation devices. Han and coworkers [3, 4, 21–28] used AUTODYN to study the separation mechanism and shock generation and shock propagation characteristics of a "ridge-cut" explosive bolt. Li [5] simulated a fragmenting-type explosive bolt by using AUTODYN to obtain critical parameters, e.g., the critical charge amount of bolt separation, internal pressure, separation time, and the speed history of a bolt body. Wang et al. [29] used LS-DYNA to analyze three different shock sources of a shear-type explosive bolt, including explosive detonation, preload release, and screw impact. Zhu et al. [30] analyzed the influence of detonation sequence and interval on the separation characteristics by establishing a SPH-FEM coupling model of several fragmenting-type explosive bolts. Huang et al. [31] analyzed the influence of preload on the output shock of a shear pin-type explosive bolt by using LS-DYNA, and the results indicated that a preload within a certain range had less effect on shock response in middle and far fields. Piston-type explosive bolts involve internal component movements, and there are few studies on their separation process and shock generation mechanism.

A piston-type explosive bolt is modeled by using a hydrocode AUTODYN in our previous research, the influence of the charge amount on separation shock are simply obtained but a detailed analysis is not performed [32]. This study was an extension of previous research. In this study, the detailed physical structure and separation characteristics test of the piston-type explosive bolt are first described. Then, the separation behavior of piston-type explosive bolts is simulated by using AUTODYN, and the fracture mechanism of an impair slot of a bolt is analyzed. The influence of the charge amount on separation time, piston speed, screw speed, and separation shock are comprehensively analyzed. Furthermore, based on the release of charge energy and the change of components energy, the influence of the charge amount on the output shock is analyzed. In the last, the propagation law of output shock of the piston-type explosive bolt on a simple aluminum plate is studied.

2. Structure and Principle

A piston-type explosive bolt (hereinafter, referred to as an "explosive bolt") is shown in Figure 1.

The explosive bolt under the study is mainly composed of an ignitor, pyrotechnic component (including charge PETN and charge cartridge), a piston, a seal ring, and a bolt body. A circumferential groove, referred to as an impair slot, is prefabricated on a side wall of a body, and its strength is greatly reduced compared to other portions. When release separation is required, the ignitor is energized to detonate the charge. The explosion shock wave and the gas product expansion jointly push the piston to break the bolt at the impair slot, thereby achieving separation.

The physical diagram of a explosive bolt before and after separation is shown in Figure 2. The bolt body after separation has no obvious deformation, and the fracture is neat without redundant fragments.

3. Separation Characteristics Test

A dynamic synchronous test system was established to measure the separation time, velocity, and output shock, as shown in Figures 3 and 4. The explosive bolts were installed in the center of a $60\,\text{cm} \times 60\,\text{cm} \times 1\,\text{cm}$ square aluminum plate suspended by four nylon ropes. To record the shock response of the explosive bolts on a test bench, three piezoresistive accelerometers (PCB 3501B1260KG, amplitude up to ±60 kg, frequency range 0–20 kHz, transverse sensitivity <3%, and resonant frequency >120 kHz) were screwed onto the bench at positions 5, 10, and 15 cm from the bench center. The sampling rate was set to 1 MHz. A 20 kHz low-pass filter was applied to the resulting accelerometer signals to reduce data aliasing during data processing.

The measurement principle is as follows: an ignition controller sends an ignition signal and ignites an ignitor. A data-acquisition system and a high-velocity camera receive the trigger signal from the ignition controller and begin working. Then, high-pressure gas pushes the piston to fracture the impair slot and releases the screw. At the same time, the generated pyroshock is transmitted to an accelerometer through an aluminum plate, and an acceleration signal is displayed on an acquisition instrument through a signal conditioner. The high-speed camera records the entire separation process, and the separation time and velocity are obtained during data processing.

3.1. Output Shock. When the charge amount is 300 mg, the collected typical acceleration histories are presented in Figure 5. The shock response spectrum (SRS) is a common method of assessing the potential of shock damage, which is the peak acceleration response of an array of a single degree-of-freedom (SDOF) system that has different natural frequencies [33]. In this study, an improved recursive digital filtering method proposed by Smowood [16] in 1981 was used to calculate the SRS. The frequency range was 100 Hz–100 kHz, the octave 1/12, and the damping ratio 0.05 (i.e., quality factor $Q = 10$). The calculation result is shown in Figure 5(b). The acceleration amplitude is greater than 20,000 G across the frequency range 100 Hz–100 kHz. The attenuation of shock occurs as the distance increases at most frequencies.

Owing to the nature of the pyroshock's high frequency, high amplitude, and short duration, the signal may be influenced by electromagnetic radiation (EMR), acoustic noise, and heat transients produced using pyrotechnic events. It is impossible to accurately analyze the separation shock characteristics of explosive bolts using these contaminated pyroshock data. In addition, if the measurement is made close to the source, such problems occur more severely. Signal anomalies also appear in this test. Although antialiasing filtering and mechanical isolation have been used, problems cannot be completely avoided. However, there is a certain safety hazard in the explosion test. The nonlinear dynamics simulation can not only avoid the above problems but also make it possible to accurately analyze many important internal dynamic parameters (such as

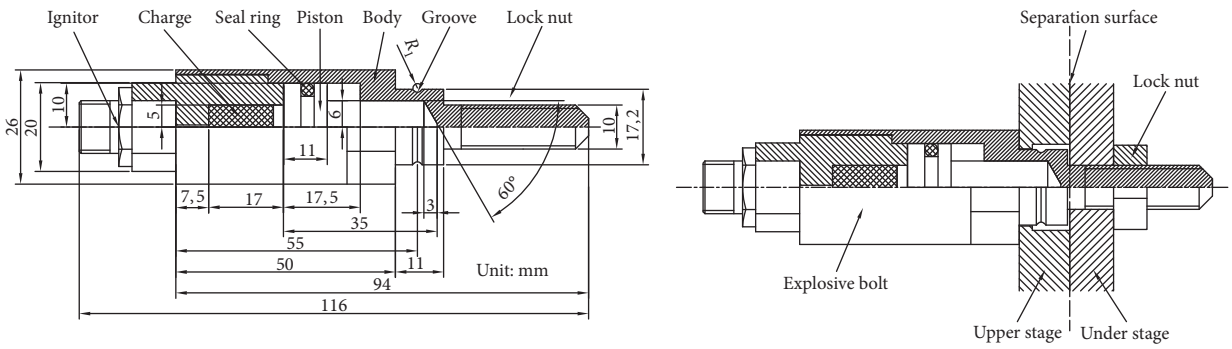

Figure 1: Schematic of a piston-type explosive bolt. (a) Structural composition and size. (b) Installation diagram.

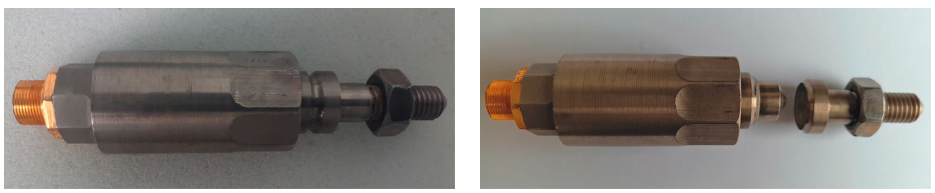

Figure 2: Photographs of the explosive bolt (a) before and (b) after separation.

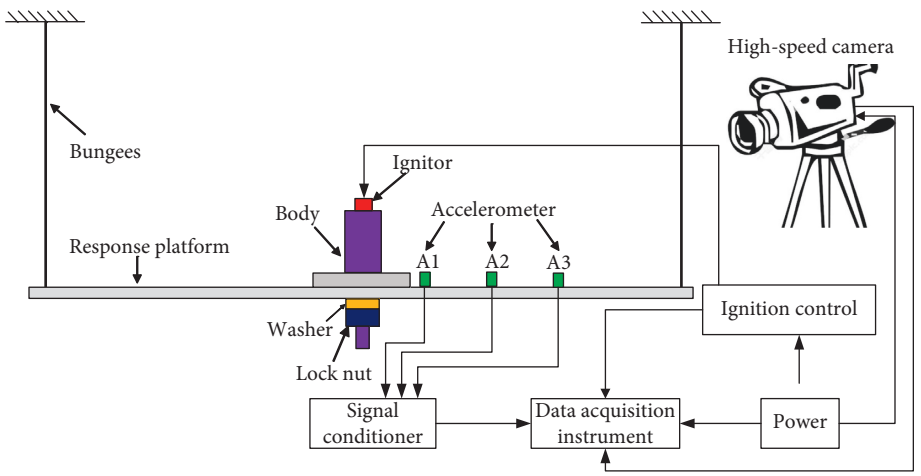

Figure 3: Diagram of separation characteristic test setup.

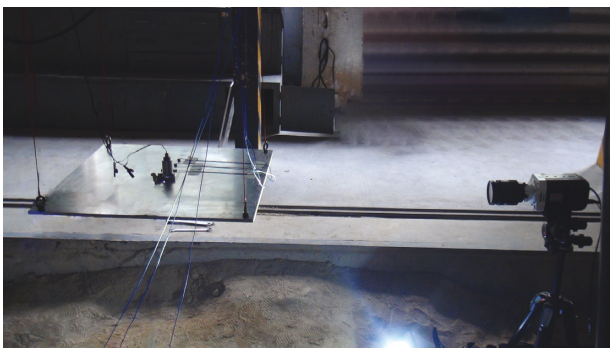

Figure 4: Measurement scene for separation characteristics.

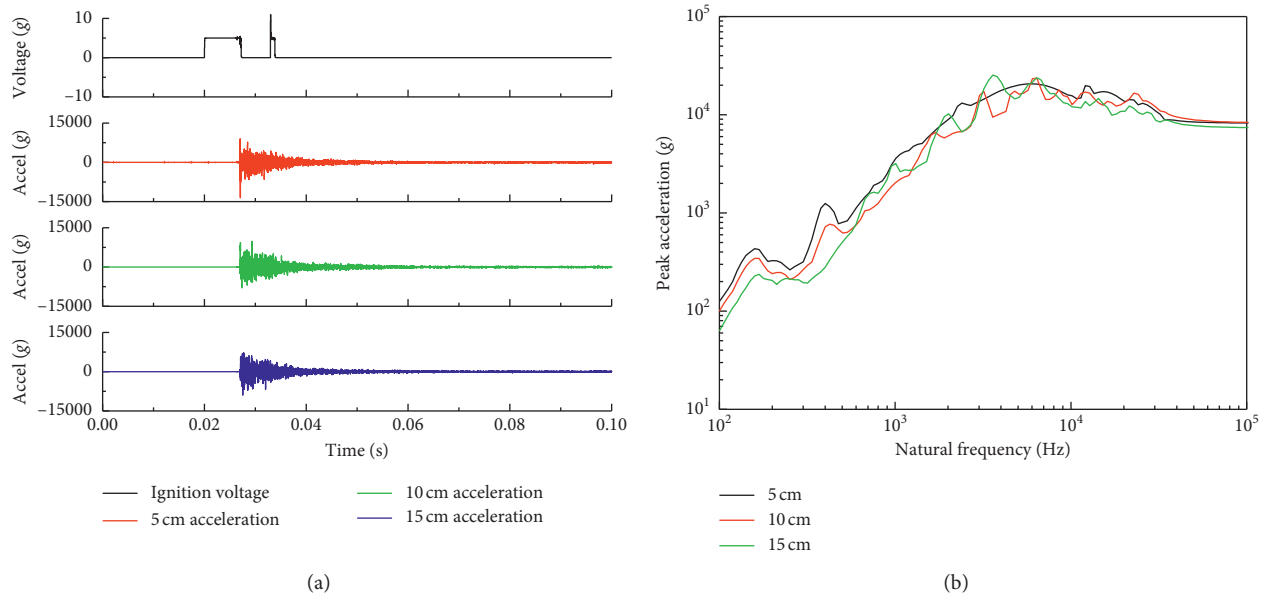

Figure 5: (a) Typical acceleration history and (b) shock response spectrum (SRS) from the experiment.

explosive pressure, stress, and energy). Based on this situation, the separation characteristics of piston-type explosive bolts were analyzed using a hydrocode AUTODYN, as discussed later in this paper.

3.2. Separation Time and Velocity. A Phantom Miro LAB310 high-speed photography system was used in this study. To obtain a resolution of 1024×768, a frame rate of 4100 frames/s and an exposure time of 185 μs were chosen for this test. High-speed photography images of two moments in the explosive bolt separation process are shown in Figure 6. The screw leaves the bolt body at 6966 μs (from triggering time), which can be approximated as the explosive bolt separation time. The separation velocity is calculated by the time difference in combination with the difference between the locations of the screw:

$$V = S_p \cdot \left(\frac{n}{\Delta t}\right), \tag{1}$$

where V is the separation velocity (m/s), S_p is the scale between the unit length and the pixel on the photograph (mm/pix), n is the number of pixels, and Δt is the time difference (μs).

The average calculated result of the separation velocity is 104 m/s. The screw velocities under different charge amounts are listed in Table 1.

4. Numerical Modeling

4.1. Physical and Numerical Models. To simplify the model, the energy generated by the combustion or explosion of primers and booster explosive is converted into a main charge (total converted amount 142 mg) and the sealing ring and others are deleted. The physical model of an explosive bolt is shown in Figure 7. The fluid-solid coupling algorithm of AUTODYN is used to compute the coupling of fluid and structure. To reduce the computational cost, a 1/4 axisymmetric model is established, as shown in Figure 8. The bolt body and piston are modeled as the Lagrange elements, and the charge and air domain are modeled as the Euler elements.

The joint numerical model of the explosive bolt and the response plate was also established according the test setup (Figure 4) to study separation shock characteristics. A series of gauge points are set on the surface parallel to the XY symmetry plane of the response plate with a 2–20 cm distance from the center of the explosive bolt. The spacing step from gauge 1 to gauge 19 is 1 cm, as illustrated in Figure 9. Only the acceleration histories of the X and Y directions were extracted at these gauge points. The acceleration time history data with a uniform time step (1 μs) were obtained by utilizing cubic spline interpolation, corresponding to a sampling rate of 1 MHz. To prevent unnecessary low-frequency drift caused by body motion (the bench only applies free boundary conditions; no bungees model is established), an eighth-order Butterworth high-pass filter with a cutoff frequency of 50 Hz was applied. Finally, the improved recursive filtering algorithm was used to calculate the SRS.

4.2. Material Model

4.2.1. Main Charge. In order to simulate the explosive detonation, the equation of state (EOS) which shows the relationship between pressure and volume must be defined. The classical trinomial EOS of Jones–Wilkins–Lee (JWL) is adopted and expressed as follows:

$$P = A\left(1 - \frac{\omega}{R_1 V}\right)e^{-R_1 V} + B\left(1 - \frac{\omega}{R_2 V}\right)e^{-R_2 V} + \frac{\omega E}{V}, \tag{2}$$

where V is the relative volume v/v_0, E is the internal energy, and A, B, R_1, R_2, and ω are the empirical parameters.

(a) (b)

Figure 6: High-speed photographs of explosive bolt separation. (a) $t = 6966\,\mu$s. (b) $t = 8186\,\mu$s.

Table 1: Material parameters of PETN.

Parameters	Value
ρ_0(g/cm^3)	0.88
A (GPa)	348.62
B (GPa)	11.288
R_1	7.0
R_2	2.0
w	0.24
D_{CJ} (m/s)	5170
P_{CJ} (GPa)	6.2
E_0 (kJ/m^3)	5.025×10^6

The specific parameters of PETN are from the AUTODYN material library and summarized in Table 1.

4.2.2. Structural Material. The materials of bolt, piston, and lock nut are 4340 stainless steel. The response plate is made of 2024 aluminum. The Johnson–Cook constitutive model is adopted to simulate their dynamic response behavior under explosive and mechanical shock. It defines the flow stress as a function of strain rate, equivalent plastic strain, and temperature. The dynamic flow stress is expressed as

$$\sigma = \left(\sigma_0 + B\varepsilon^n\right) + \left(1 + C \ln \frac{\dot{\varepsilon}}{\dot{\varepsilon}_0}\right) + \left[\left(1 - \left(\frac{T - T_r}{T_m - T_r}\right)\right)^m\right], \tag{3}$$

where σ is the flow stress, σ_0 is the static yield stress, B is the hardening constant, ε is the strain, n is the hardening exponent, C is the strain rate constant, $\dot{\varepsilon}$ is the strain rate, $\dot{\varepsilon}_0$ is the reference strain rate, T is the temperature, T_r is the reference temperature, T_m is the melting point, and m is the thermal softening exponent.

The Johnson–Cook failure model is also used to describe the piston (4340 steel) failure. The computational damage parameter "D" is based on damage buildup and is given by

$$D = \sum \frac{\Delta\varepsilon^p}{\varepsilon^f}, \tag{4}$$

where D is the damage to the material element, $\Delta\varepsilon^p$ is the increment of accumulated plastic strain, ε^f is the accumulated plastic from stress triaxiality, temperature, and strain rate and is defined as

$$\varepsilon^f = \left[D_1 + D_2 e^{D_3\sigma^*}\right]\left[1 + D_4 \ln \frac{\dot{\varepsilon}}{\dot{\varepsilon}_0}\right]\left[1 + D_5 \frac{T - T_r}{T_m - T_r}\right], \tag{5}$$

where ε^f is the failure strain; σ^* is the ratio of mean stress to equivalent stress; D_1, D_2, D_3, D_4, and D_5 are constants; and the others are the same as the Johnson–Cook strength model. Failure occurs when the facture parameter "D" reaches the value of 1.

In addition, in order to describe the relationship between pressure and volume of structure materials under shock, the shock EOS is utilized, which is the Mie–Grüneisen form of EOS that uses the shock Hugoniot as reference:

$$P - P_H = \frac{\gamma}{\nu}\left(e - e_H\right), \tag{6}$$

where P is the pressure, γ is the Grüneisen constant, ν is the specific volume, and e is the specific internal energy. Subscript H denotes the shock Hugoniot, which is defined as the locus of all shocked states for each material. Here, shock EOS needs the P–ν Hugoniot, which can be obtained from the U–u Hugoniot or the relationship between shock and particle velocities:

$$U = C_0 + su, \tag{7}$$

where C_0 and s are the empirical parameters.

All material parameters are taken from the AUTODYN material library. The specific parameters of 4340 stainless steel and 2024 aluminum are listed in Tables 2 and 3, respectively.

4.2.3. Air. The air in the Euler grids is described by using the ideal gas state equation, which is

$$P = (\gamma - 1)\rho E, \tag{8}$$

where γ is the adiabatic exponent (for the ideal gas, $\gamma = 1.4$); ρ is the density, and the initial density of air is 0.001225 g/cm^3; and E is the gas specific thermodynamic energy, and the initial value E_0 is 2.068×10^5 J/kg.

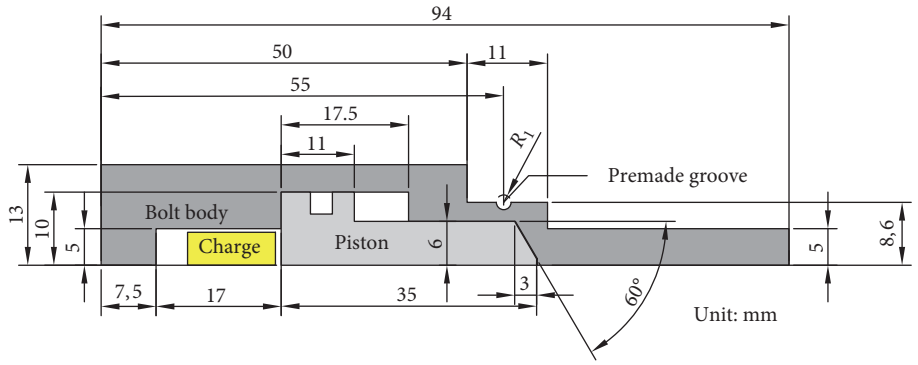

Figure 7: Simplified physical model of the explosive bolt.

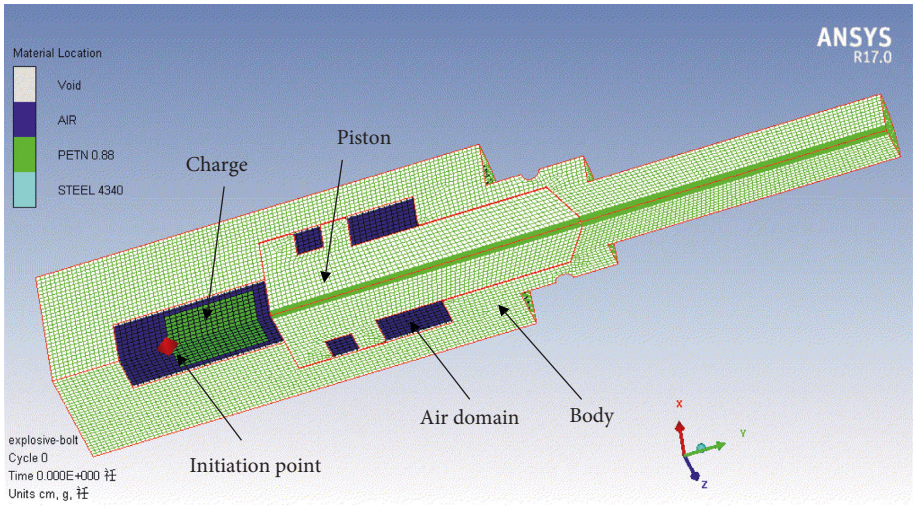

Figure 8: Numerical model of the explosive bolt.

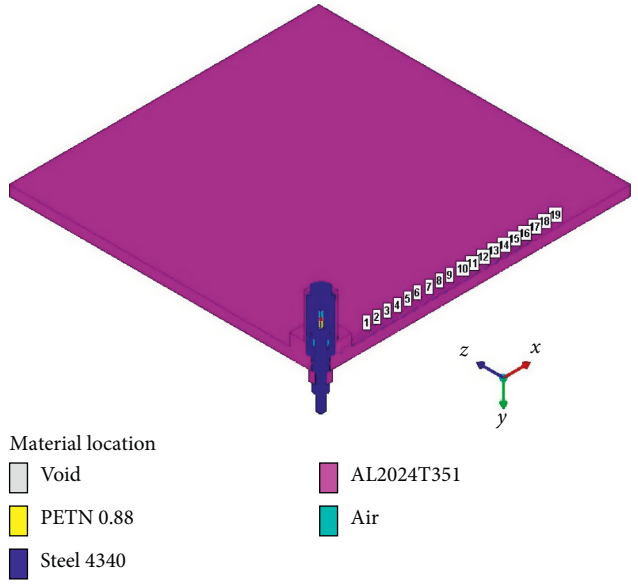

Figure 9: Separation shock analysis models of the explosive bolt.

Table 2: Material parameters of 4340 stainless steel.

Shock EOS		Johnson–Cook strength model		Johnson–Cook failure model	
ρ_0 (g/cm3)	7.83	σ_0 (GPa)	0.792	D_1	0.05
γ	1.77	B (GPa)	0.51	D_2	3.44
C_0 (m/s)	3382	n	0.26	D_3	−2.12
S_1	1.812	C	0.014	D_4	0.002
T_r (K)	300	m	1.03	D_5	0.61
C_p (J/kg·K)	477	T_m (K)	1793	Erosion criterion	
		$\dot{\varepsilon}_0$ (s^{-1})	1.0	Type	Failure

Table 3: Material parameters of 2024 aluminum.

Shock EOS		Johnson–Cook strength model	
ρ_0 (g/cm^3)	2.785	σ_0 (GPa)	0.265
γ	2.00	B (GPa)	0.426
C_0 (m/s)	5328	n	0.34
S_1	1.338	C	0.015
T_r (K)	300	m	1.00
C_p (J/kg·K)	875	T_m (K)	775
		$\dot{\varepsilon}_0$ (s^{-1})	1.0

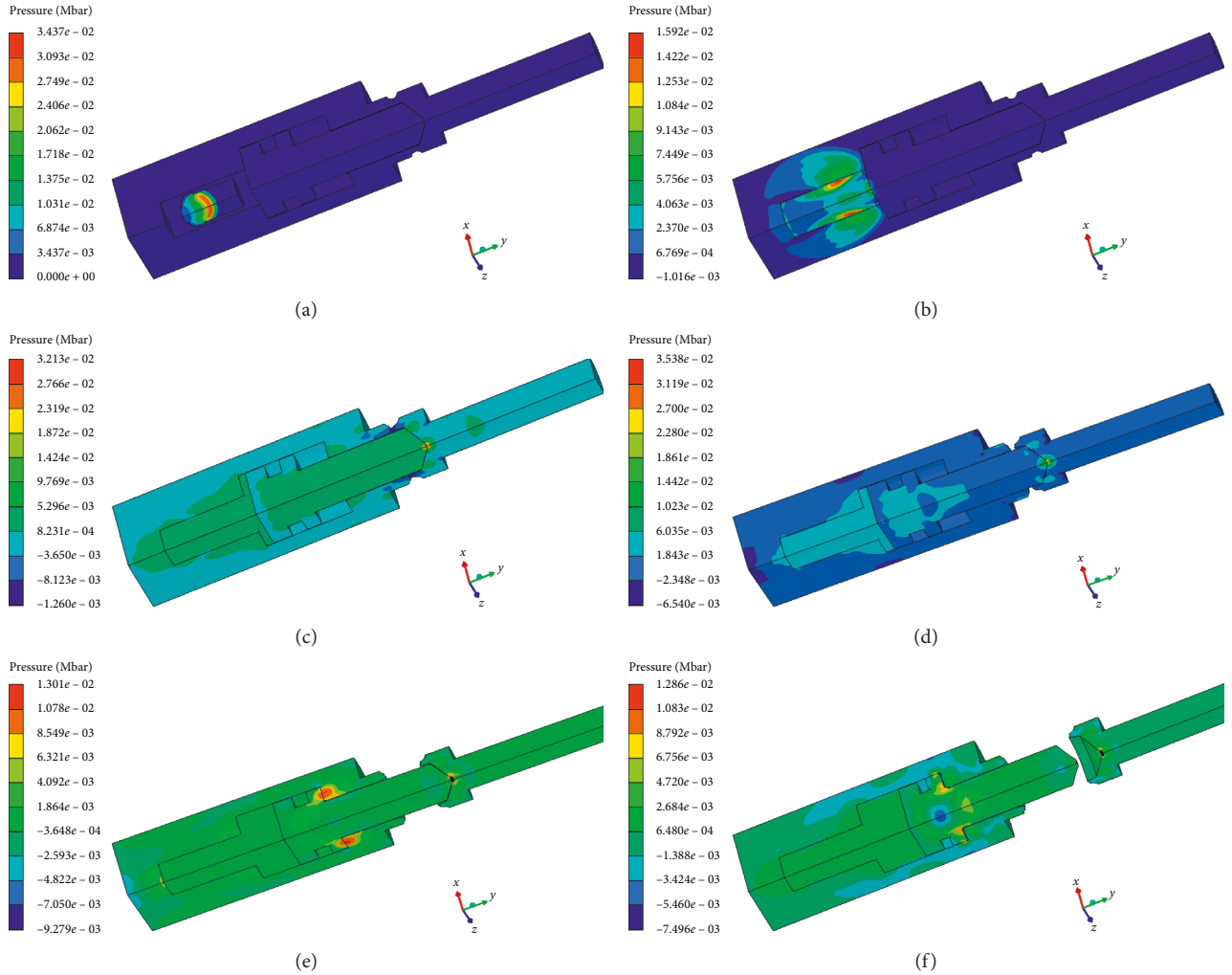

Figure 10: Pressure contours of the explosive bolt separation process. (a) $t = 1\,\mu s$, (b) $t = 3\,\mu s$, (c) $t = 70\,\mu s$, (d) $t = 83\,\mu s$, (e) $t = 155\,\mu s$, and (f) $t = 200\,\mu s$.

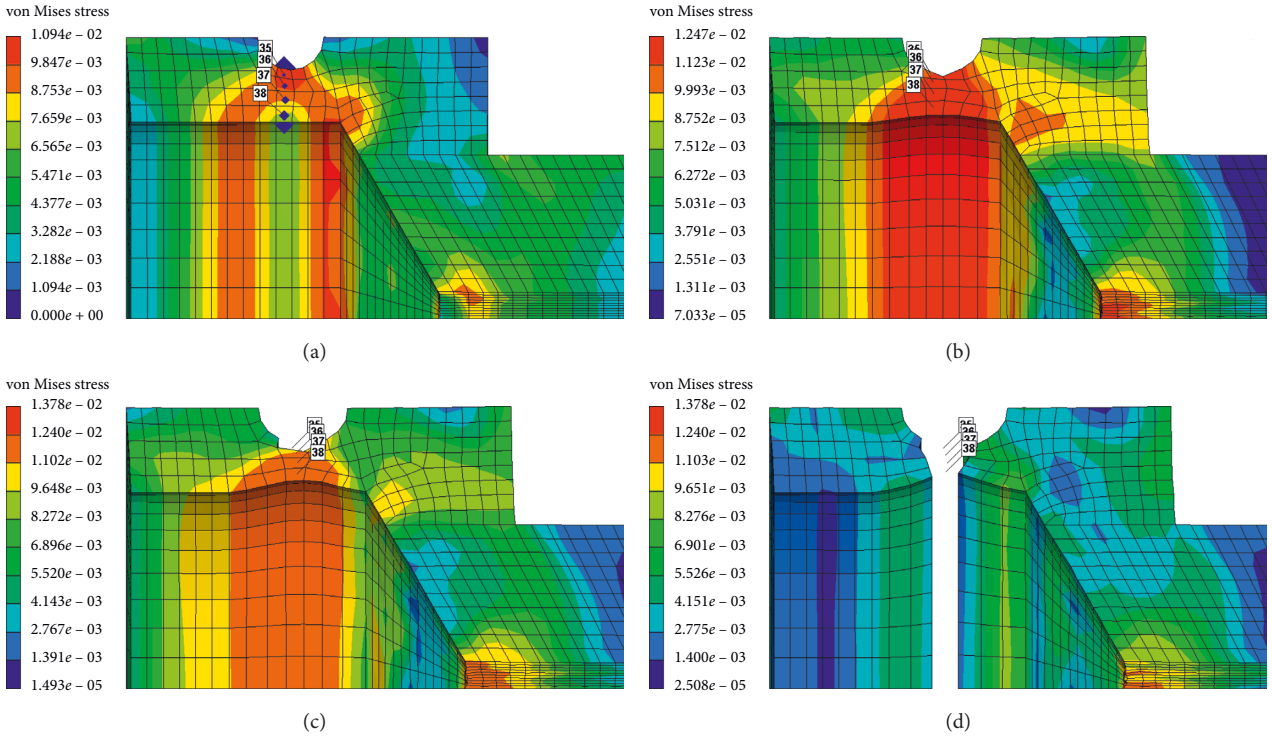

Figure 11: von Mises stress contours on the impair slot. (a) $t = 15\,\mu$s, (b) $t = 58\,\mu$s, (c) $t = 70\,\mu$s, and (d) $t = 83\,\mu$s.

5. Results and Analysis

5.1. Separation Processes. The pressure contours of the explosive bolt during separation processes are shown in Figure 10. At $0\,\mu$s, the charge was detonated. Then, the propagation of detonation waves and expansion of products started at $1\,\mu$s, as shown in Figure 10(a). The shock waves propagated reached the end face of the piston, and the products filled the entire chamber at approximately $3\,\mu$s, as shown in Figure 10(b). Then, the shock wave and expansion of products drove the piston to move forward, and a tensile stress was formed at the pregroove. The pregroove reached the failure criterion and began to fail at approximately $70\,\mu$s, as shown in Figure 10(c). At $83\,\mu$s, the failure expanded radially along the groove, eventually forming a fracture and starting separation, as shown in Figure 10(d). As the fracture was formed, the piston accelerated forward and released the screw. At $155\,\mu$s, the piston hit the body shoulder, and the velocity instantaneously decreased and eventually stopped moving, as shown in Figure 10(e). When the piston stopped moving, the screw was no longer subjected to the loading force and kept flying at a constant speed to complete the separation, as shown in Figure 10(f).

5.2. Fracture Mechanism of Impair Slot. The von Misses stress contour of the explosive bolt is shown in Figure 11. It can be seen from Figure 11(a) that the stress concentrated on the impair slot due to the loading from the piston. Then, elements of the impair slot reached the yield point and resulted in necking, as shown in Figure 11(b). At $70\,\mu$s, the stress at the tip of the groove exceeded the critical value of the dynamic fracture limit and began to crack, as shown in Figure 11(c). The cracks expanded along the radial direction, and the impair slot was completely broken, as shown in Figure 11(d). Therefore, the separation of the impair slot of the bolt is mainly caused by the tensile fracture mechanism.

To deeply analyze the dynamic fracture characteristics of the bolt body, the von Mises stress, effective plastic strain, and damage histories of the four typical elements at the impair slot were monitored, and the results are shown in Figure 12. At approximately $15\,\mu$s, the stress of the outer tip of the impair slot (Gauge 35) first reached the yield limit and yielding occurred. The plastic strain and damage began to increase slowly, while the stress oscillated during the yielding stage. At approximately $30\,\mu$s, the materials entered the strengthening phase, the stress increased again, and the strain and damage increased significantly. At approximately $70\,\mu$s, the element of Gauge 35 was deleted due to failure (the damage value reaches 1), and its stress and strain rapidly decreased to zero. At approximately $83\,\mu$s, the innermost element of Gauge 38 was also broken, and the bolt was completely broken. In addition, due to the dynamic strain rate effects of the material, the maximum value of the equivalent stress is greater than the static fracture limit of the material, which is approximately 1220 MPa, as shown in Figure 12(a). There is a difference in the maximum plastic strains of the four typical elements because the failure criterion is defined as the cumulative damage factor D (equation (4)). It is the ratio of accumulated plastic strain increment divided by failure plastic strain, which takes into account the effects of stress state, strain rate, and temperature.

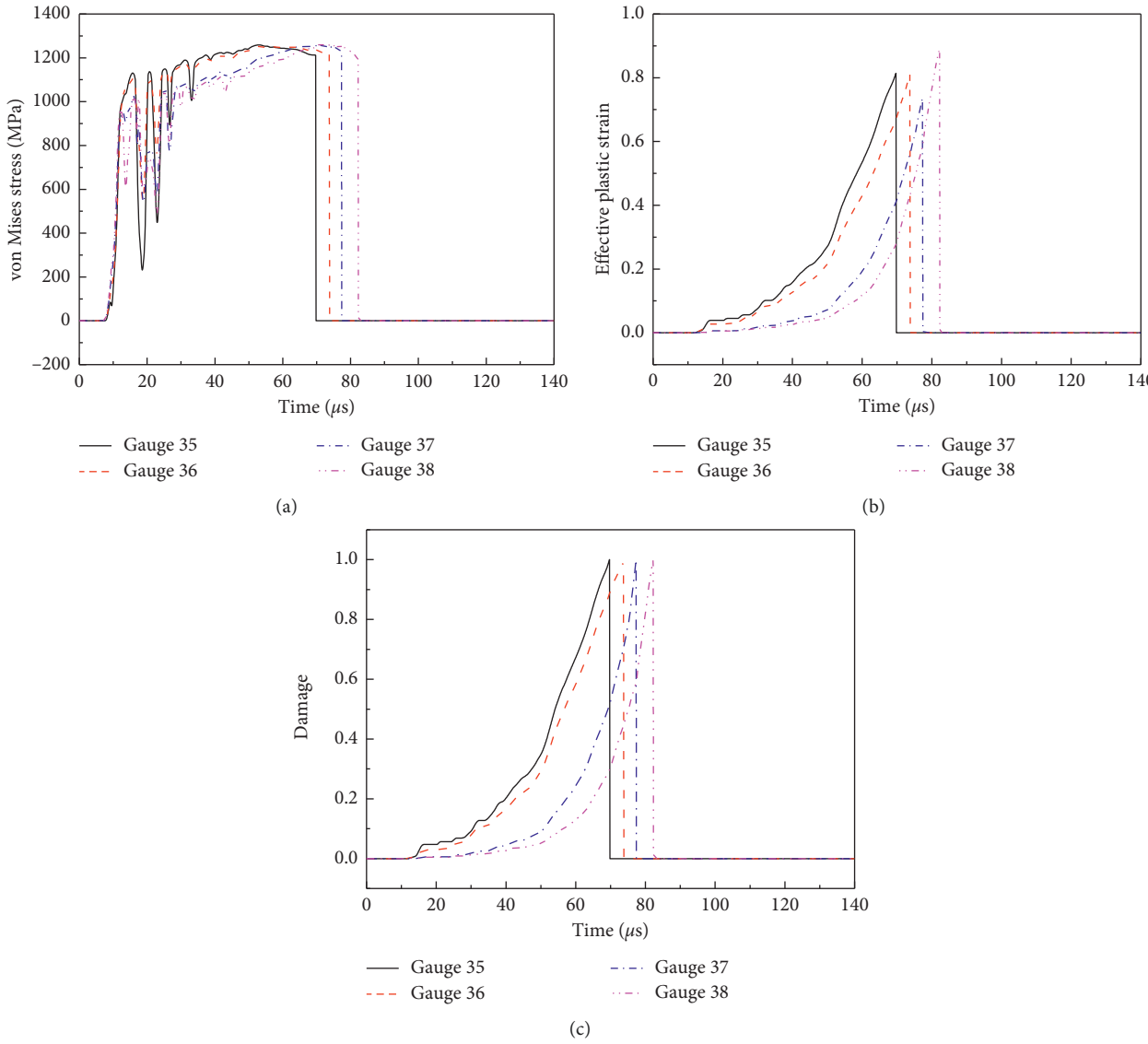

Figure 12: (a) von Mises stress; (b) effective plastic strain; (c) damage histories on the impair slot.

5.3. Analysis of Shock Sources. When the charge amount was 442 mg, the shock acceleration history and response spectrum in the X and Y directions 2 cm from the source are as shown in Figure 13. It can be clearly seen from the acceleration history that there are two distinct peaks. Combined with the simulation of the separation process in Section 4.1, it can be seen that the two peaks are caused by the pyrotechnic explosion and piston impact.

To verify this judgment, the acceleration history in the X direction at 2 cm under 354 and 442 mg is plotted in Figure 14, which shows that the former obviously does not have a second peak because it does not achieve separation and there is no piston impact process, which will be explained in Section 5.5 below.

In addition, it can be seen that the shock response in the Y direction is significantly larger than that in the X direction. This is because Y is the main direction of the explosion shock wave propagation and piston impact.

5.4. Comparison of Simulation and Experiment. Because of the simplification of the structure and the inability of the material model to fully express the real material behavior, there are some deviations in the simulation results. Moreover, due to the randomness of the charge amount, structural materials, and manufacturing, the experiment results also have some randomness. In addition, it has been stated in Section 3.1 that the pyroshock signal in the test may also be affected by electromagnetic radiation (EMR), acoustic noise, and heat transients produced using pyrotechnic events. Therefore, the deviation between the simulation and experiment results is inevitable. The tolerances most commonly used in current aerospace practice are specified for the maximax SRS and shall be used: ±6 dB when the natural frequency is less than 3 kHz and +9/6 dB when the natural frequency is greater than 3 kHz [14, 15]. In order to simplify and be strict, the former is adopted uniformly in this paper. The shock

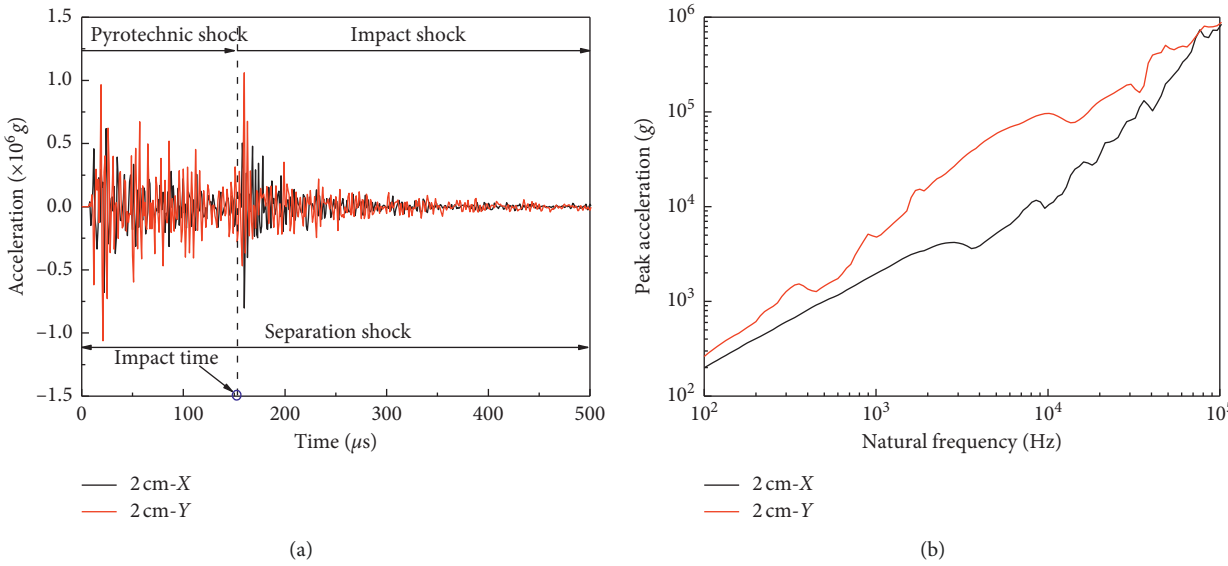

Figure 13: Separation shock in X and Y directions at 2 cm under 442 mg. (a) Acceleration history. (b) SRS.

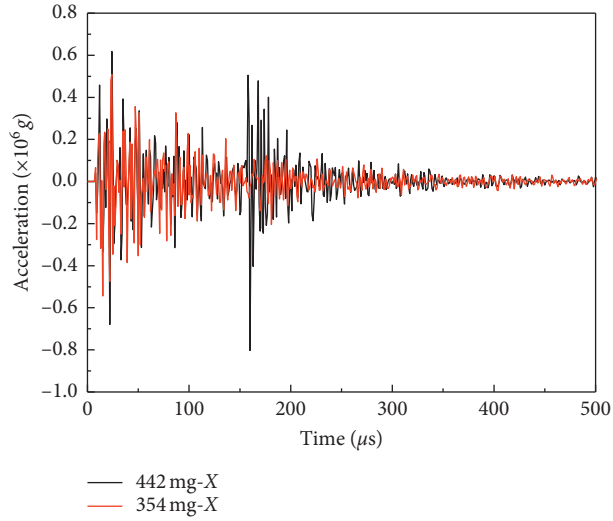

Figure 14: Acceleration in the X direction at 2 cm under 354 and 442 mg.

response spectra obtained by simulation and experiment at 5, 10, and 15 cm are compared in Figure 15. The experimental SRS is enveloped using ±6 dB of the simulated SRS, except for the individual frequencies, which indicates that the simulation model can predict the separation shock of explosive bolts.

5.5. Effects of Charge Amount on Separation Time and Velocity. From the analysis of separation shock source in Section 5.3, it is known that the peak velocity of a piston has a great influence on a separation shock. The variation law of the velocity of the piston and the screw during the separation process under a 442 mg charge amount is analyzed, and the results are shown in Figure 16. The piston velocity first increased to approximately 20 m/s under the action of the detonation shock wave and product expansion. Then, the front end of the body was loaded to stretch the impair slot. At approximately 70 μs, the impair slot began to fracture, the velocity of the piston increased sharply, and finally the body was broken. The velocity of the piston reached a peak when the piston moved to the maximum stroke. The speed then decreased sharply when the piston hit the body shoulder. However, due to the deformation of the body caused by the impact, the piston continued to move forward for a distance until it stopped. Before the fracture of the impair slot, the velocity of the screw was small. When the fracture of the impair slot occurred, the velocity of the screw increased sharply until it was completely separated from the piston.

The velocities of the piston and screw were calculated for different charge amounts, and the results are shown in Figures 17 and 18, respectively.

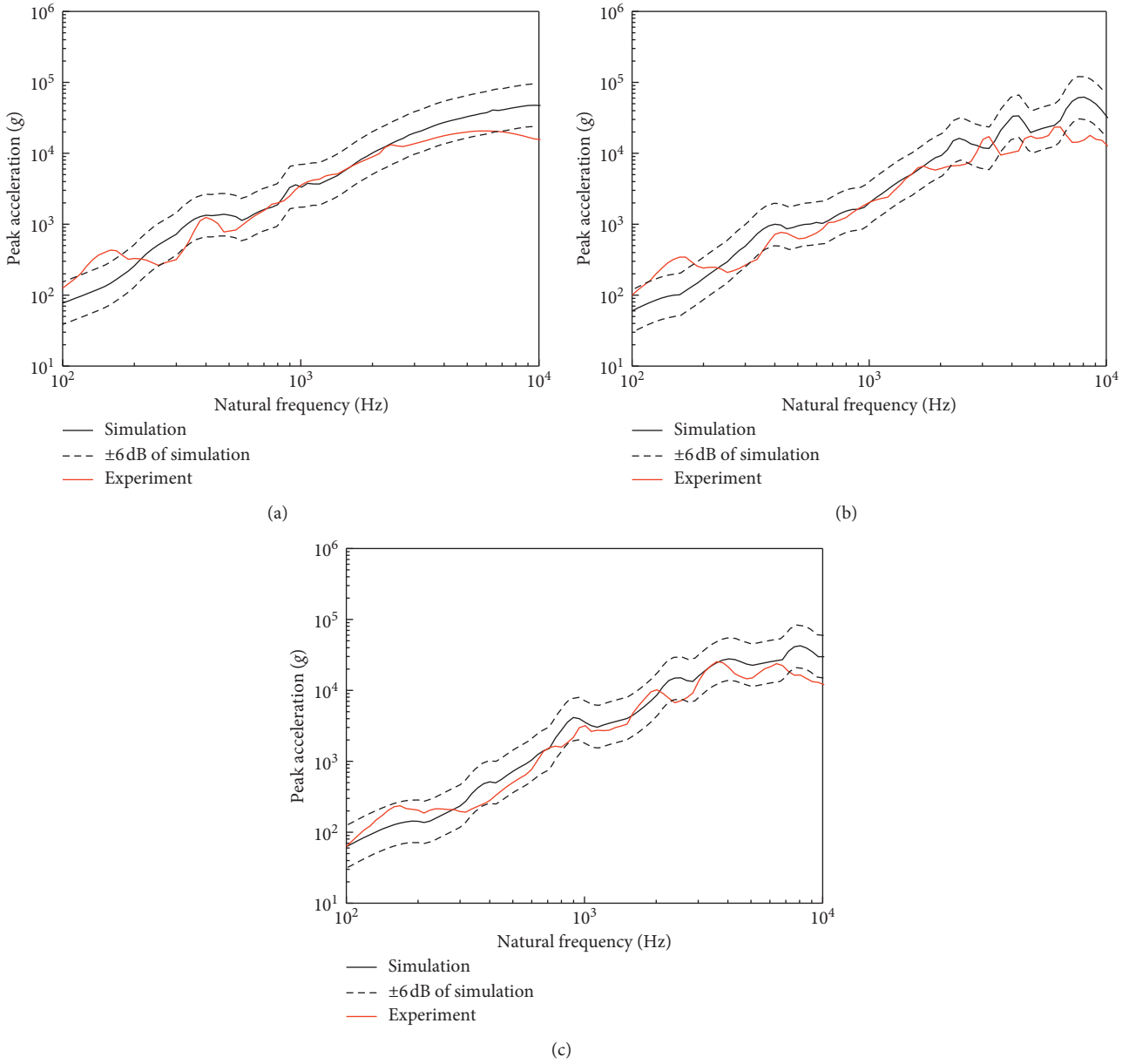

Figure 15: Comparison of SRS levels between simulation and experiment [32]. (a) 5 cm. (b) 10 cm. (c) 15 cm.

It can be seen from Figure 17 that the piston velocity in the early stage increased as the charge amount increased, but the velocity of the piston collision did not continue to increase. The piston collision speeds under different charge amounts are listed in Table 1, and the separation time (defined as the time when the bolt is completely broken, unlike in the actual test, which does not include the ignition delay time), the screw fly out speed, and the experimentally measured screw speed are also listed. Combined with the piston speed history (Figure 17), at a 354 mg charge amount, the product pressure was not sufficient to push the piston to break the body. The piston speed was only a small step caused by the initial shock wave, and then the oscillation dropped to 0. When it was broken, the piston exhibited an acceleration phase. Its collision speed first increased and then decreased with the charge, reaching a maximum when the charge amount was 531 mg.

To analyze the reason for this, the piston displacement curves for different charge amounts are plotted in Figure 19. When the design stroke of the piston is fixed, the overall velocity of the piston is larger as the charge is increased, and the collision time is advanced so that the collision velocity does not necessarily increase. In addition, it can be seen from Table 4 that the final screw speed obtained by the simulation is close to the test value, and the error is less than 10%.

5.6. Effects of Charge Amount on Separation Shock. The acceleration of the main direction (Y direction) at different distances from the source was extracted under different charge amounts, and the corresponding SRS was calculated.

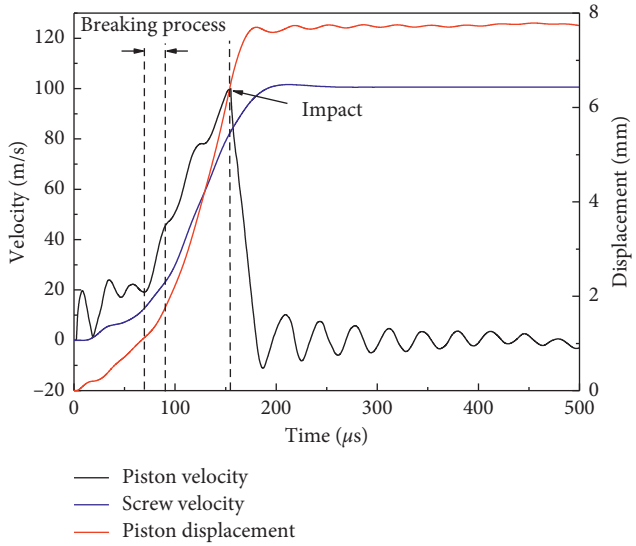

Figure 16: Velocity histories of the piston and screw at 442 mg charge amount.

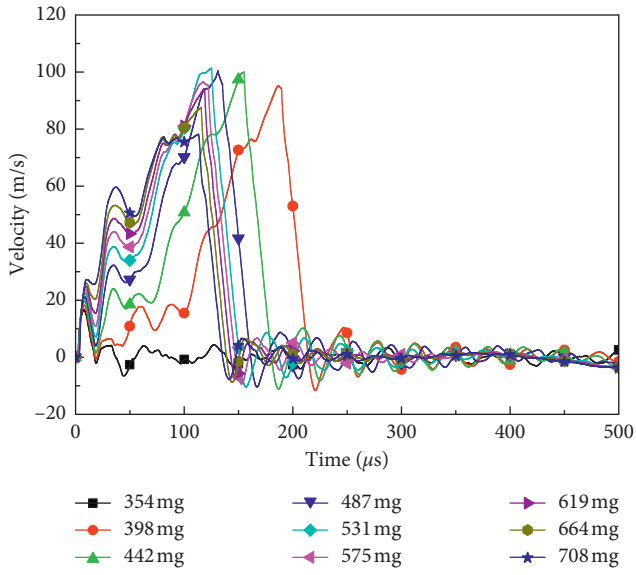

Figure 17: Velocities of the piston under different charge amounts.

The SRS levels (at 2 cm) at three typical charge amounts are shown in Figure 20.

It can be seen that the SRS levels generally increase with increasing charge amount, but this rule is not always met in each frequency range. Two dimensionless coefficients of M_r and E_r that do not consider the frequency were defined to better study the influence of the charge and are expressed as follows:

$$M_r = \frac{\mathrm{Max}\left(\mathrm{SRS}_a(f)\right)}{\mathrm{Max}\left(\mathrm{SRS}_b(f)\right)},$$
$$E_r = \frac{\sum_{f=f_0}^{f_N} \mathrm{SRS}_a(f)}{\sum_{f=f_0}^{f_N} \mathrm{SRS}_b(f)}, \quad (9)$$

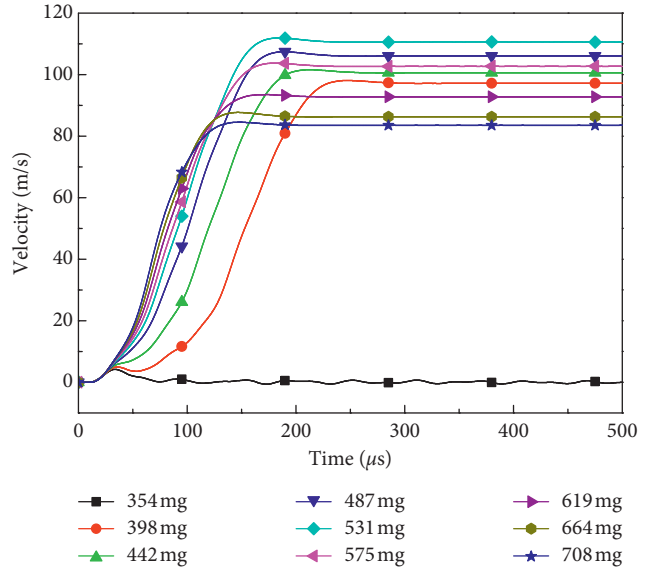

Figure 18: Velocities of the screw under different charge amounts.

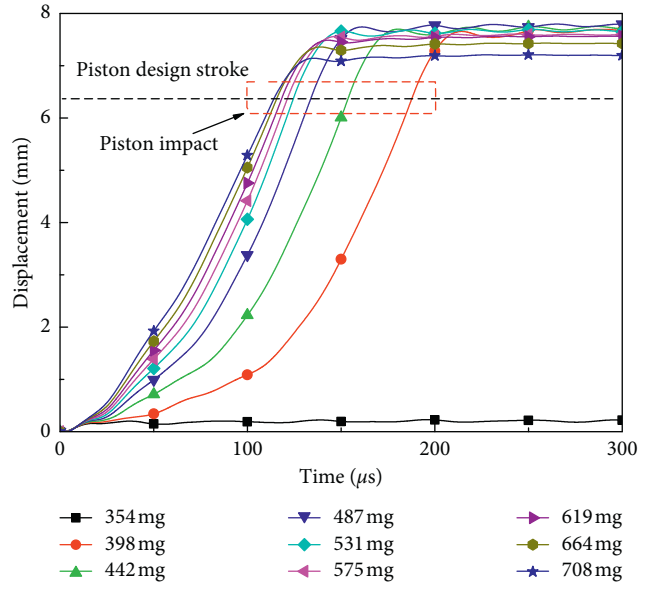

Figure 19: Displacements of the piston under different charge amounts.

where M_r is the maximum relative coefficient of the SRS and E_r the average relative coefficient of the SRS in the entire frequency domain. $\mathrm{SRS}_b(f)$ is the reference SRS. Here, the reference SRS is the SRS of the 442 mg charge amount in the Y direction at 2 cm.

The M_r and E_r values at four locations were calculated and are shown in Figure 21.

It can be seen from Figure 21 that the influence of the charge amount on the shock is not a simple linear relationship in terms of M_r or E_r. The explosive bolts are not separated at 310 and 354 mg. Their separation shocks are basically consistent except for the near field 2 cm. Since the shock in the unseparated condition is only caused by the

Table 4: Separation characteristics of explosive bolts under different charge amounts.

Charge amount (mg)	Separation time (μs)	Peak velocity of piston (m/s)	Peak velocity of screw (m/s)	Velocity of screw from the test (m/s)	Difference (%)
310			No separation		
354			No separation		
398	111	95.2	97.2	No test	—
442	83	100.0	100.6	96	4.8%
487	69	100.5	106.1	102	4.0%
531	64	101.3	110.6	116	4.7%
575	61	96.6	102.7	97	5.9%
619	59	94.3	92.7	87	6.6%
664	57	87.5	86.3	No test	—
708	54	78.2	83.5	No test	—

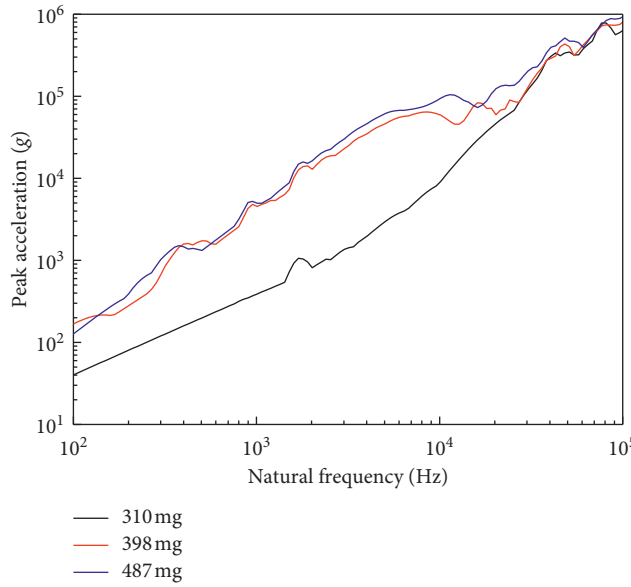

Figure 20: SRS levels at three typical charge amounts.

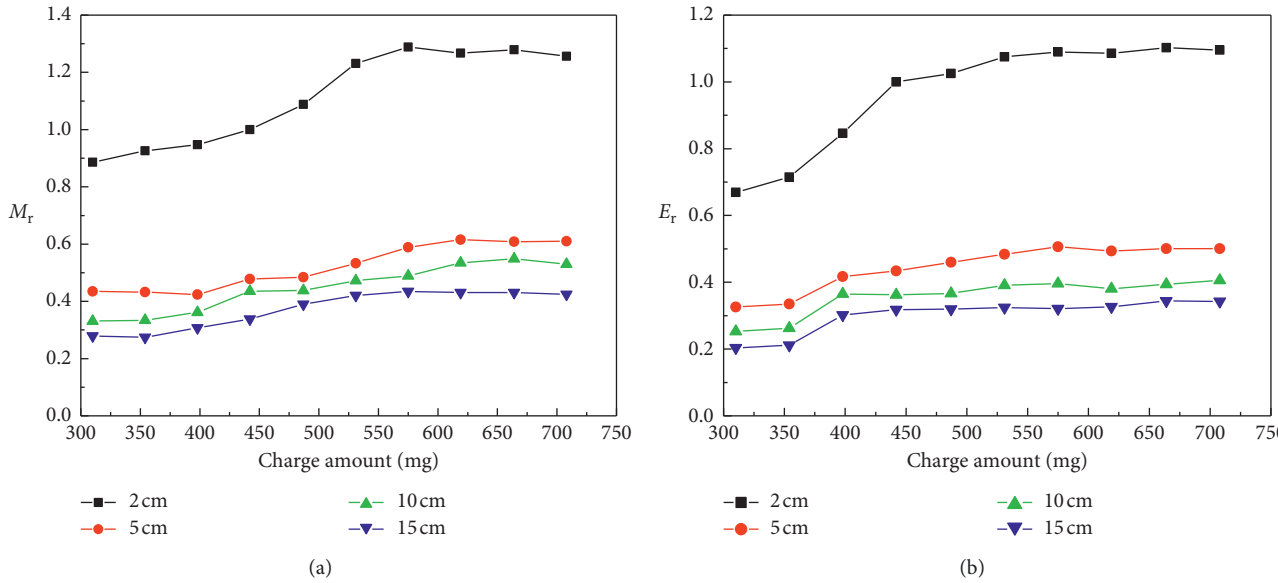

Figure 21: Relationship curves between SRS and charge amount [32]. (a) Maximum coefficient. (b) Mean coefficient.

explosion shock wave, the shock wave dissipates quickly as the distance increases. The near-field region is directly affected by the shock wave, while the far-field shock response is mainly dominated by the stress wave and structural resonance. When the charge amount was increased from 354 to 398 mg, the separation shock sharply increased because the explosive bolts achieved separation and the shock caused by the piston impact was introduced. In the case of separation, the separation shock first increased with increasing charge amount and then tended to stabilize at 531 mg. Although the explosion shock increased as the charge amount increased, the shock caused by the decrease in the impact speed of the piston decreased.

The combined result of the two causes resulted in an output shock that remained essentially unchanged.

Next, the cause of this phenomenon was analyzed from the perspective of energy conversion. The energy histories of the key components during the separation process are shown in Figures 22–25 at 442 mg. Combined with the simulation of the separation process discussed in Section 4.1, there are several important moments that were considered: I ($t = 70\,\mu s$), II ($t = 83\,\mu s$), III ($t = 155\,\mu s$), and IV ($t = 180\,\mu s$). Moment I refers to the moment the bolt started to break, moment II to the moment the bolt was completely broken, moment III to the moment the piston collided with the shoulder of the body, and moment IV to the moment the piston stopped.

Because the heat dissipation is not considered in the simulation, during the separation process, the combustion or detonation of the charge converts its internal energy into the internal energy and kinetic energy of the external structure, such as the body, the piston, and the response plate.

Before moment I, the internal energy of the piston and body exhibited a rising phase due to the explosion deformation. During the process of bolt breaking (moments I–II), the internal energy of the body slightly decreased due to some element failures being deleted, while the kinetic energy of the piston and the body increased slightly due to the slight increase in speed. The internal energy of the piston was basically unchanged, and the internal energy of charge was slightly decreased. After the bolt was completely broken (moments II–III), the internal energy of the charge decreased rapidly, while the kinetic energy of the piston increased rapidly due to the expansion of the product pushing the piston to work. The speed of the front part of the body (also called the screw) increased due to the loading of the piston, so the kinetic energy of the body also increased. In this process, both the body and the piston were substantially no longer deformed, so their internal energy was substantially unchanged. When the piston hit the shoulder (moment III) of the body, the piston converted the kinetic energy into the deformed internal energy of the body and the piston. The kinetic energy of the piston decreased sharply to zero, and the internal energy of the piston and the body increased sharply. When the piston impact was stabilized (moment IV), the energy conversion essentially stopped.

The energy history of the response plate was analyzed based on the results plotted in Figure 25. Before the body

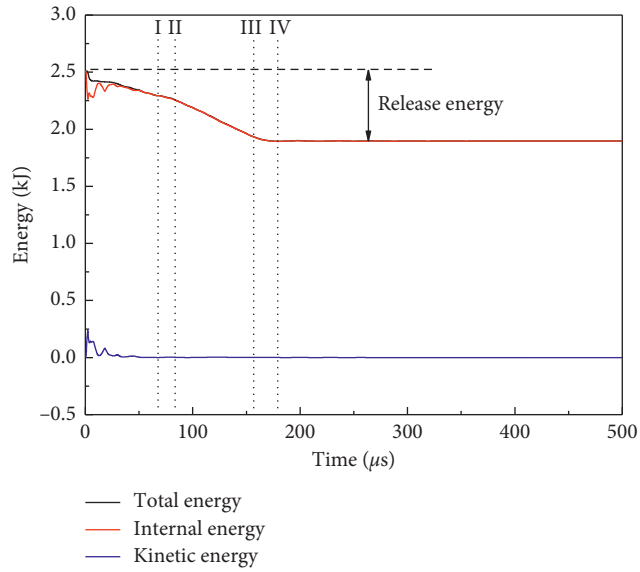

Figure 22: Energy histories of 442°mg charge amount.

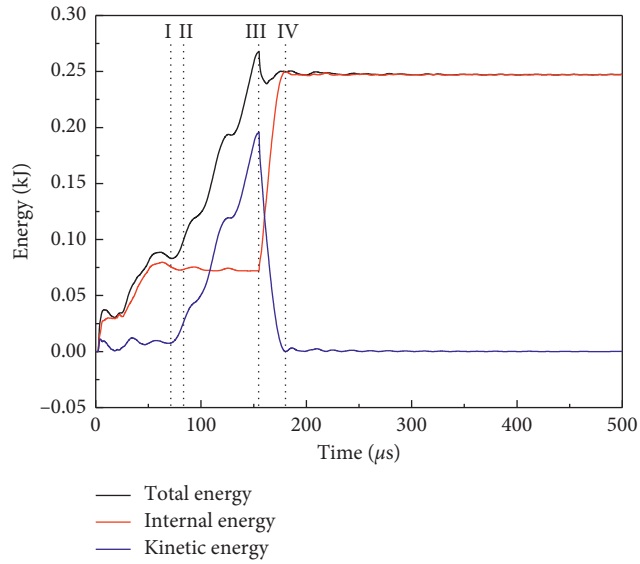

Figure 23: Energy histories of the piston at 442°mg charge amount.

fracture (moment II), the internal energy and kinetic energy of the response plate increase were relatively small, mainly resulting from the transfer of the body and piston. After the bolt was completely broken (moments II–III), the kinetic energy and internal energy of the response plate increased sharply. When the piston hit the shoulder of the body (moment III), the kinetic energy of the piston also turned into the internal energy of the response plate through the shoulder of the body, and the response plate slightly increased. After the impact was stabilized (moment IV), the internal energy and kinetic energy of the response plate decreased with fluctuations due to stress wave reflection, structural resonance, and structural damping.

Using the same method, the peaks of the charge energy (total energy, internal energy, and kinetic energy) and the

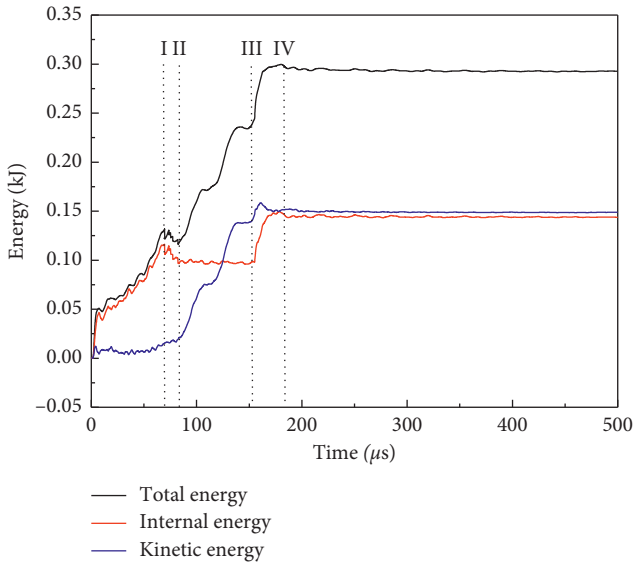

Figure 24: Energy histories of the body at 442°mg charge amount.

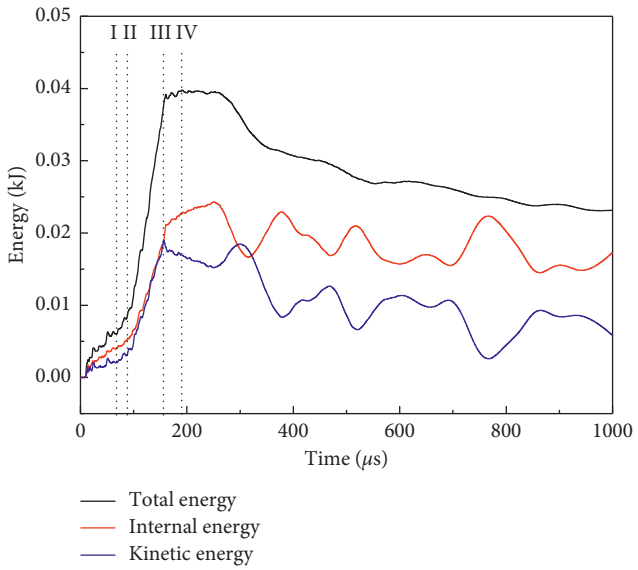

Figure 25: Energy histories of the response plate at 442°mg charge amount.

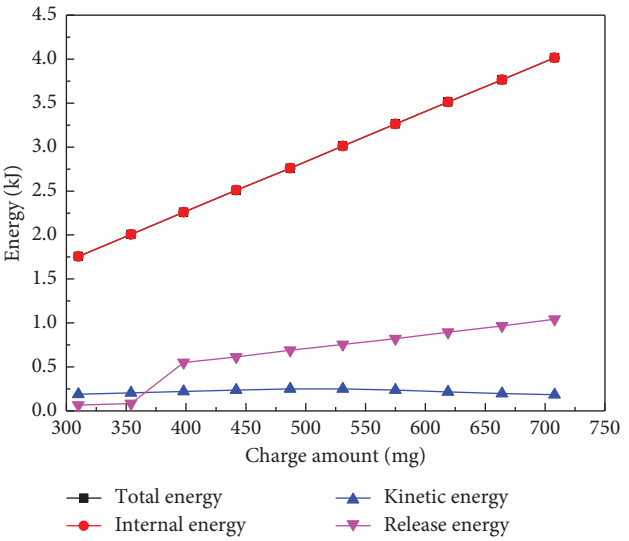

Figure 26: Peak energy curves of the charge amount.

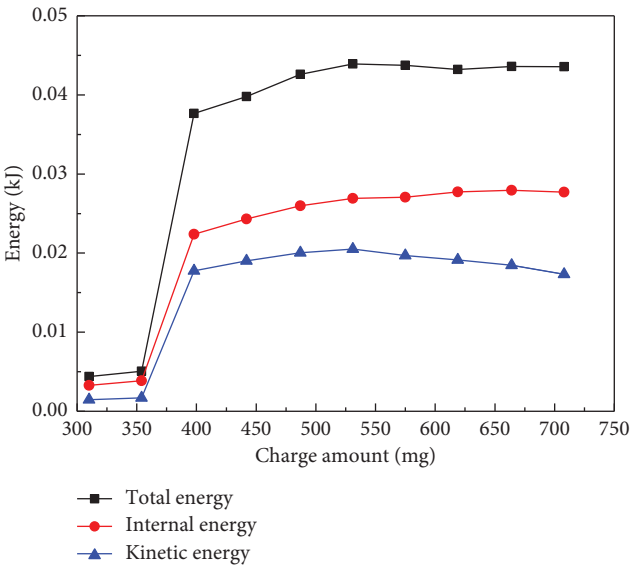

Figure 27: Peak energy curves of the response plate.

release energy of charge, as well as the peaks of energy (total energy, internal energy, and kinetic energy) of the response plate, were obtained under different amounts of charge, as shown in Figures 26 and 27. Combined with the analysis of the relationship between charge amount and separation shock (Figure 21), we found the following. When separation was not achieved (310 and 354 mg), their charge release energies were basically the same, and the separation shock was also basically consistent because the energy difference obtained using the response plate was small. When the charge amount increased from 354 to 398 mg, the energy released by the charge and the energy obtained by the response plate increased sharply due to the piston hitting the body so that the separation shock response also increased sharply. In the case of separation, the energy released from the charge increased linearly as the charge increased, and the kinetic energy of the response plate first increased and then decreased. Furthermore, the internal energy continued to increase, eventually first increasing and then remaining constant. This behavior corresponds to the shock response law.

5.7. Shock Attenuation with Distance. To analyze the distance attenuation characteristics of the separation shock propagation, we took the explosive bolt 442°mg charge amount as an example. We extracted the acceleration in the X and Y directions at different distances on the response plate and calculated the corresponding SRS. The acceleration history and response spectra for the four typical locations (2, 5, 10, and 15 cm) are shown in Figures 28 and 29, respectively. In any direction, the SRS value generally decreased with increasing distance, but this law is not always satisfied at each

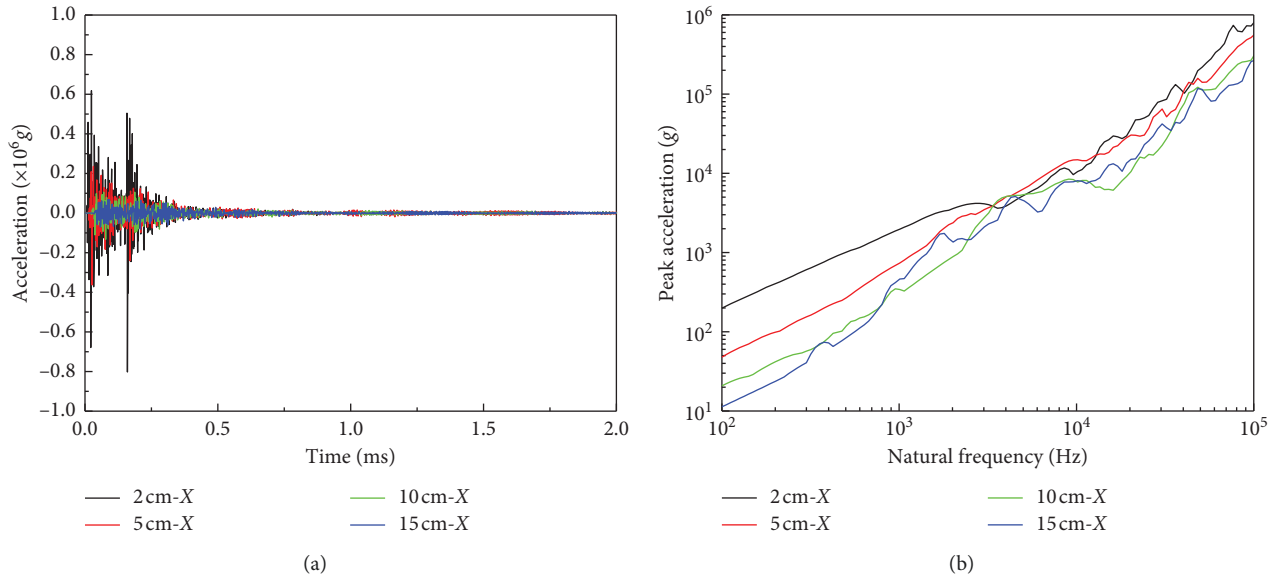

Figure 28: Separation shock in the X direction at four different locations. (a) Acceleration history. (b) SRS.

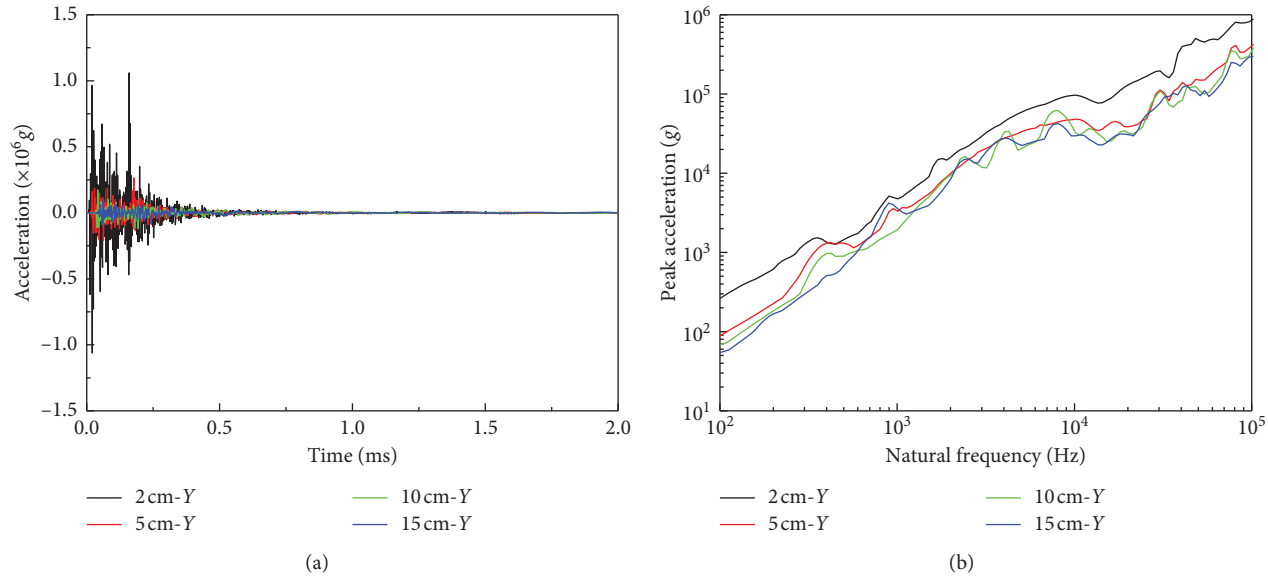

Figure 29: Separation shock in the Y direction at four different locations. (a) Acceleration history. (b) SRS.

frequency. Using the same method detailed in Section 5.6, the SRS at 2 cm at a 442°mg charge amount was used as a reference SRS, and the two relative coefficients of the SRS at different distances in the X and Y directions were calculated, and the results are plotted in Figure 30.

Overall, as the distance increased, both coefficients showed a decreasing trend. In addition, certain dispersion is manifested, especially on the maximum relative coefficient, which is mainly due to contact, friction, and nonlinear characteristics of the material. To establish the distance attenuation model of the separation shock, the relationships between the two coefficients and the distance are fitted, and the fitting equation is a power function:

$$M_r \text{ or } E_r = a \cdot d^b, \tag{10}$$

where d is the distance from the center of the impact source and a and b are constants.

The fitting results in both X and Y directions are shown in Tables 5 and 6 and the fitting curve in Figure 30.

The results show that M_r and E_r decreased as the distance increased. The attenuation rate of SRS gradually tended to be stable and obeyed the power function law. In the X direction, the shock response at 5 cm was attenuated by approximately 30% compared with that at 2 cm and was attenuated by approximately 60% in the Y direction (main shock direction). This means that the equipment should not be

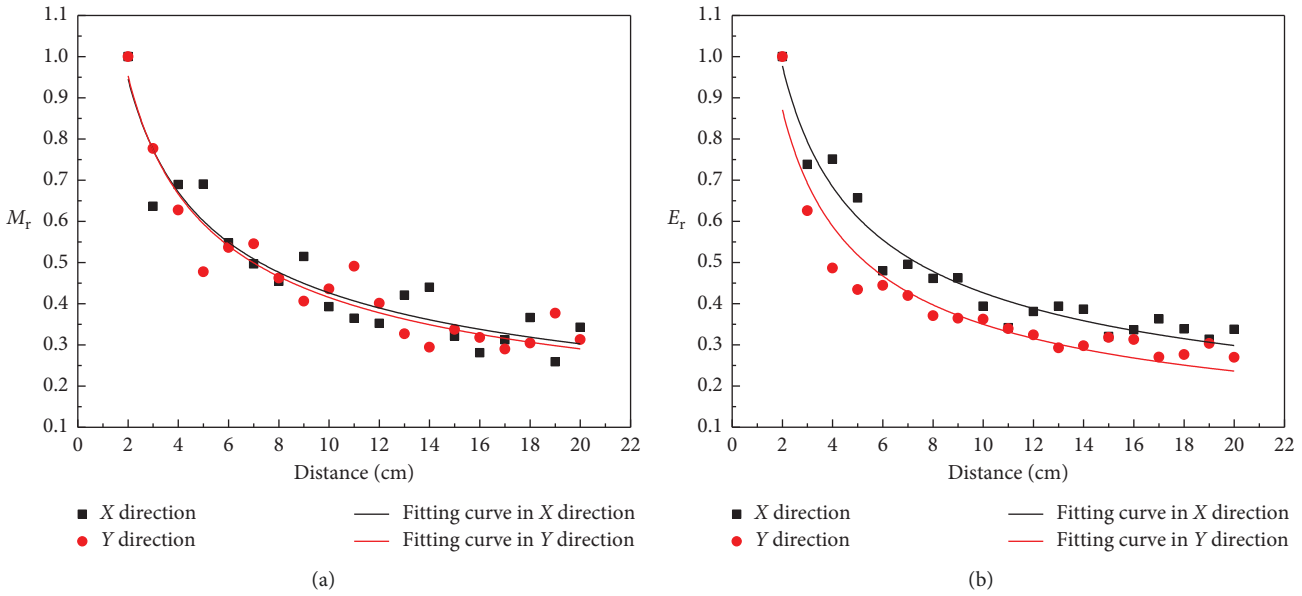

Figure 30: Relationship curves between SRS and distance. (a) Maximum coefficient. (b) Mean coefficient.

Table 5: Fitting coefficient of M_r and distance.

Direction	Coefficient a	Coefficient b	R^2
X	1.33265	−0.49483	0.89729
Y	1.36316	−0.51617	0.92569

Table 6: Fitting coefficient of E_r and distance.

Direction	Coefficient a	Coefficient b	R^2
X	1.39707	−0.51527	0.95327
Y	1.28997	−0.56658	0.90128

installed in the vicinity of the impact source, which can provide reference for the installation and protection of the equipment.

6. Conclusions

In the work described in this paper, the structure and working principle of a piston-type explosive bolt were first introduced, and the separation and output shock experiments are carried out. Then, the whole separation process of the piston-type explosive bolt is simulated with the hydrocode AUTODYN, using the fluid-solid coupling algorithm. The numerical model is verified by comparing the measure point SRS of simulation with experimental results. The influence of the charge amount on separation time, separation speed, and separation shock are analyzed. The numerical simulation reveals that the separation mechanism of the piston explosive bolts is the dynamic tensile fracture mechanism and that the critical charge amount for separation is 354–398 mg of PETN. Under the constant stroke of the internal piston, as the charge amount increases, the bolt separation time decreases, while the collision speed of the piston first increases and then decreases, reaching a maximum at 531 mg. The analysis of the output shock acceleration history shows that the pyrotechnic explosion and piston impact are the main sources of separation shock of the piston explosive bolt. By calculating two relative dimensionless values (maximum relative coefficient M_r and the average relative coefficient E_r) of the shock response spectrum, it is indicated that the separation shock first increases with the increase of the charge amount and then stabilizes after 531 mg. The cause of this phenomenon is explained by analyzing the release of charge energy and the change of components energy. In addition, on a simple aluminum plate, the shock response decreases with increasing distance from the shock source, obeying the power function attenuation law.

Data Availability

The simulation and test data used to support the findings of this study are available from the corresponding author upon request.

Conflicts of Interest

The authors declare no conflicts of interest regarding the publication of this paper.

Acknowledgments

We thank LetPub (http://www.letpub.com) for its linguistic assistance during the preparation of this manuscript. This work was supported by the joint fund of the National Natural Science Foundation of China and the China Academy of Engineering Physics (Grant no. U1530135).

References

[1] L. J. Bement and M. L. Schimmel, *A Manual for Pyrotechnic Design*, Development and Qualification, NASA, Hampton, VA, USA, 1995.

[2] Z. S. Liu, X. J. Wang, X. C. Zhu, and G. H. Wang, *Aerospace Pyrotechnic Devices*, Chinese Astronautics Press, Beijing, China, 2012.

[3] J. Lee, D. H. Hwang, and J. H. Han, "Numerical study on pyroshock generation and propagation from pyrotechnic release devices using hydrocodes," in *Proceedings of 21st International Congress on Sound and Vibration*, pp. 1–8, Florence, Italy, July 2015.

[4] Y. J. Lee, "The interpretation of separation mechanism of ridge-cut explosive bolt using simulation programs," *Journal of the Society of Magnetic Resonance in Medicine*, vol. 56, no. 2, pp. 395–410, 2004.

[5] Y. Li, *The Structural, Design and Numerical Analysis of Explosive Bolt with Impair Slot*, Nanjing University of Science and Technology, Nanjing, China, 2010.

[6] Y. H. Li, X. G. Li, Y. Q. Wen, S. W. Guo, L. Cheng, and H. N. Mu, "Optimal design of an explosive separation device based on LS-DYNA," *Journal of Beijing Institute of Technology*, vol. 25, pp. 24–28, 2016.

[7] H. L. Liu, D. L. Cui, and S. Z. Yan, "Numerical simulation of the dynamic fracture of no-contamination explosive bolts," *Journal of Tsinghua University (Science and Technology)*, vol. 55, no. 3, pp. 292–297, 2015.

[8] T. Y. Ye, Y. Wang, X. F. Wang, and J. Zhang, "Discussion on the design of an explosive separation device based on LS-DYNA," *Journal of Beijing Institute of Technology*, vol. 25, pp. 24–28, 2016.

[9] Y. H. Li, S. H. Xiong, Y. Li et al., "Identification of pyrotechnic shock sources for shear type explosive bolt," *Shock and Vibration*, vol. 2017, Article ID 3846236, 9 pages, 2017.

[10] C. T. Hou, W. Yi, T. Tang, K. L. Rong, and B. J. Ma, "Strength study on a typical explosive bolt," *Structure & Environment Engineering*, vol. 25, no. 4, pp. 11–14, 2007.

[11] C. J. Moening, *Pyrotechnic Shock Flight Failures*, Institute of environmental sciences pyrotechnic shock tutorial program in 31st Annual Technical Meeting, Washington, DC, USA, 1985.

[12] S. J. Gentz, D. O. Ordway, D. S. Parsons, C. M. Garrison, C. S. Rodgers, and B. W. Collins, *Empirical Model Development for Predicting Shock Response on Composite Materials Subjected to Pyroshock Loading*, NASA, Washington, DC, USA, 2015.

[13] W. O. Hughes and A. M. McNelis, *Statistical Analysis of a Large Sample Size Pyroshock Test Data Set Including Post Flight Data Assessment*, NASA, Washington, DC, USA, 1998.

[14] M. G. Ryschkewitsch, *Pyroshock Test Criteria*, NASA, Washington, DC, USA, 2011.

[15] DOD, *Pyroshock, MIL-STD-810G Method 517.1*, Department of Defense, New York, NY, USA, 2008.

[16] IEST, *Pyroshock Testing Techniques*, Institute of Environmental Science and Technology, Schaumburg, IL, USA, 2009.

[17] PLA, *Laboratory Environmental Test Methods for Military Materiel-Part 27: Pyroshock Test*, The Chinese People's Liberation Army in the Equipment Department, Beijing, China, 2009.

[18] J.-R. Lee, C. C. Chia, and C.-W. Kong, "Review of pyroshock wave measurement and simulation for space systems," *Measurement*, vol. 45, no. 4, pp. 631–642, 2012.

[19] H. Zhang, T. X. Liu, C. J. Li, S. H. Xiang, and Q. M. Zhang, "Status and application analysis of spacecraft pyroshock protection techniques," *Spacecraft Engineering*, vol. 23, no. 2, pp. 104–113, 2014.

[20] H. Zhang, C. J. Li, T. X. Liu et al., *Review of Spacecraft Pyroshock Reduction Technique*, The Academic Seminar on Reliability Technology of Machinery Industry, 2013.

[21] J. Lee, J.-H. Han, Y. Lee et al., "Separation characteristics study of ridge-cut explosive bolts," *Aerospace Science and Technology*, vol. 39, no. 39, pp. 153–168, 2014.

[22] J. Lee, J.-H. Han, Y. Lee et al., "A parametric study of ridge-cut explosive bolts using hydrocodes," *International Journal of Aeronautical and Space Sciences*, vol. 16, no. 1, pp. 50–63, 2015.

[23] J. Lee, J. H. Han, Y. J. Lee et al., "Design of low-shock ridge-cut explosive bolts based on separation behavior analysis," in *Proceedings of 40th International Pyrotechnic Seminar*, pp. 44–56, Colorado Springs, USA, July 2014.

[24] J. Lee, D. H. Hwang, J. K. Jang et al., "Pyroshock prediction of ridge-cut explosive bolts using hydrocodes," *Shock and Vibration*, vol. 2016, Article ID 1218767, 14 pages, 2016.

[25] S. J. Lee, D. H. Hwang, and J. H. Han, "Development of pyroshock simulator for shock propagation test," *Shock and Vibration*, vol. 2018, Article ID 9753793, 13 pages, 2018.

[26] J. Lee, D.-H. Hwang, and J.-H. Han, "Study on pyroshock propagation through plates with joints and washers," *Aerospace Science and Technology*, vol. 79, pp. 441–458, 2018.

[27] J. Lee, D. H. Hwang, J. K. Jang, J. R. Lee, and J. H. Han, "Nondestructive evaluation of pyroshock propagation using hydrocodes," in *Proceedings of Active and Passive Smart Structures and Integrated Systems*, pp. 1–8, Las Vegas, NV, USA, March 2016.

[28] J.-K. Jang and J.-R. Lee, "Nondestructive prediction of point source pyroshock response spectra based on experimental conditioning of laser-induced shocks," *Optics & Laser Technology*, vol. 61, pp. 24–33, 2014.

[29] J. P. Wang, Y. J. Mao, and H. J. Huang, "Numerical simulation for impulsively loading mechanism of a point pyrotechnic separation device," *Journal of Vibration and Shock*, vol. 32, no. 2, pp. 9–13, 2013.

[30] D. J. Zhu, W. H. Chu, D. L. Liang, and S. P. Wang, "Characteristics of a vehicle's pyroshock based on SPH-FEM coupled method," *Journal of Vibration and Shock*, vol. 34, no. 11, pp. 68–74, 2015.

[31] H. J. Huang, J. P. Wang, Y. J. Mao, X. H. Yue, and J. Lv, "Influence of pretightening force of explosive bolts on impulse response," *Journal of Vibration and Shock*, vol. 34, no. 16, pp. 166–169, 2015.

[32] Y. H. Li, J. C. Wang, L. Cheng et al., "Numerical simulation of separation shock characteristics of a piston type explosive bolt," *Vibroengineering PROCEDIA*, vol. 21, pp. 214–219, 2018.

[33] A. G. Piersol, T. L. Paez, and C. M. Harris, *Harris's Shock and Vibration Handbook*, McGraw-Hillm, New York, NY, USA, 6th edition, 2010.

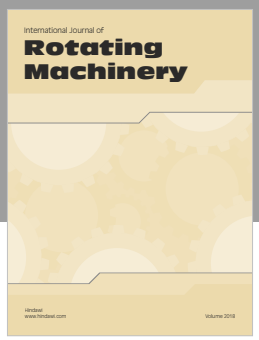

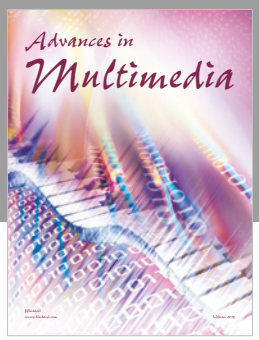

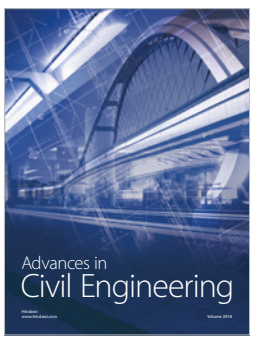

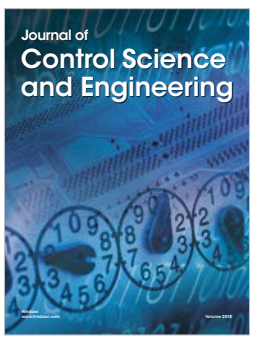

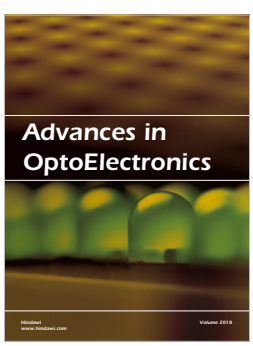

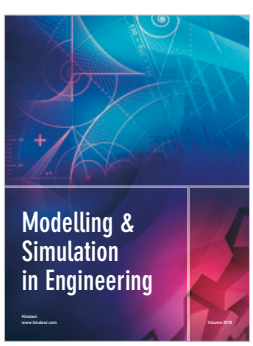

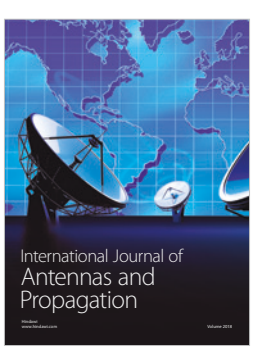

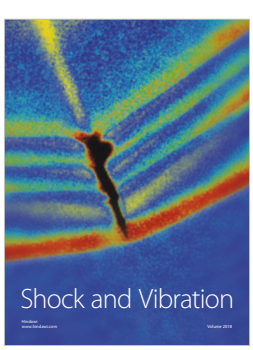

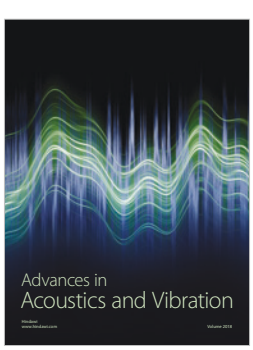

Hindawi

Submit your manuscripts at
www.hindawi.com